

DOI: 10.1002/cplu.201300380

Synthesis of Carbon Materials–TiO₂ Hybrid Nanostructures and Their Visible-Light Photo-catalytic Activity

Qian Li,^[a] Juncao Bian,^[b] Li Zhang,^[c] Ruiqin Zhang,^[b] Guozhong Wang,^[d] and Dickon H. L. Ng^{*[a]}

Activated carbon, graphene, carbon nanotubes and fullerene were incorporated into TiO₂ by a solvothermal approach and thermal annealing to produce carbon materials–TiO₂ hybrid nanostructures. The carbon materials–TiO₂ products were characterised by using SEM, TEM, XRD, Raman spectroscopy, X-ray photo-electron spectroscopy, UV-visible spectroscopy and photo-luminescence. The aim was to study the interactions between the main TiO₂ phase and the carbon components, and the relationships between morphology, structure and photo-degradation of the rhodamine B (RhB) dye. An enhanced photo-catalytic degradation of RhB was achieved when using

these nanocomposites over that for only using pure TiO₂. The superiority in photo-catalytic activities on the RhB molecules resulted from contributions from the excellent adsorption property, favourable chemical bond formation (Ti–O–C), narrower band gap, smaller particle size and effective charge-carrier separation of the nanocomposites. Compared with the graphene-, carbon nanotube- and fullerene–TiO₂ products, activated carbon–TiO₂ exhibited weaker interactions between carbon and titania, lower adsorption for RhB and a larger band gap, which led to lower photo-catalytic activity of RhB.

Introduction

Energy crisis and environmental deterioration are by-products of industrialisation. As a remedy, photo-catalysis has been widely employed to deal with air and water treatment.^[1] It is known that anatase titania (TiO₂) is a promising photo-catalytic candidate material owing to its photo-stability, non-toxicity, relatively high catalytic performance and low cost.^[2] However, anatase TiO₂ suffers from rapid electron–hole recombination, which leads to low photo-catalytic efficiency.^[3] Moreover, TiO₂ has a wide band gap (3.2 eV) and is only active under UV-light irradiation, although UV radiation only makes up 5% of normal sunlight.^[4] To use sunlight to activate TiO₂, measures have to be taken to broaden visible-light harvesting and retard the recombination process of electron–hole pairs for anatase after their generation. Some approaches such as non-metal

doping,^[5] metal doping,^[6] coupled semiconductor^[7] and noble-metal-based composites^[2a,8] have been investigated. In addition, mesoporous hollow TiO₂ structures with high crystallinity and surface areas,^[2b,c] TiO₂ nanorod,^[1b] and TiO₂ nanotubes,^[9] were prepared in an effort to enhance mass transfer between the active sites and to favour isolation between active sites of the catalyst and the dye molecules.

Recently, photo-catalysts containing carbon components have attracted a great deal of attention owing to their superior adsorption ability for pollutants in addition to their photo-catalytic activities.^[4,10] For example, an activated carbon (AC) component with a porous structure can provide a large specific surface area for adsorption and, at the same time, serves as a support to the catalyst.^[11] This type of product will increase catalyst adsorption performance to pollutants as well as facilitate mass transfer during the photo-catalytic reaction. Another example is that owing to the unique electric and structural properties of carbon nanotubes (CNTs), which have high conductivity, large specific surface area and strong adsorption capability. CNTs were considered to be suitable dopants for the catalyst to enhance photo-catalysis.^[4] One interesting report was that CNTs had a large electron-storage capacity (one electron per 32 carbon atoms), and thus, could serve as excellent electron acceptors.^[12] Xu et al. synthesised CNT/TiO₂ nanocomposites, which were utilised to degrade gas-phase benzene, by using a simple impregnation method.^[13] The functions of CNTs were multi-fold, for example, one CNT could act as electron traps to prolong the lifetime of the created electron–hole pairs and the other acted a dispersing agent to control the morphology of the nanocomposite. The formation of Ti–C and Ti–O–C bonds on the surface of CNT–TiO₂ film would narrow the

[a] Q. Li, Prof. D. H. L. Ng
Department of Physics
The Chinese University of Hong Kong
Shatin (Hong Kong)
Fax: (+852) 39436392
E-mail: dng@phy.cuhk.edu.hk

[b] J. Bian, Prof. R. Zhang
Department of Physics and Materials Science
and Centre for Functional Photonics (CFP)
City University of Hong Kong (Hong Kong)

[c] Prof. L. Zhang
Department of Mechanical and Automation Engineering
The Chinese University of Hong Kong (Hong Kong)

[d] Prof. G. Wang
Institute of Solid State Physics
Chinese Academy of Sciences
Anhui (P. R. China)

 Supporting information for this article is available on the WWW under <http://dx.doi.org/10.1002/cplu.201300380>.

band gap of the nanocomposite.^[4] In another study it was shown that, for fullerene (C_{60}), with a high electron affinity and a Fermi level located below the conduction band (CB) of TiO_2 , its photo-generated electron would be energetically favoured to flow from the CB of TiO_2 to C_{60} .^[3] It is also known that graphene (GR) and reduced graphene oxide (GO) are outstanding species among the carbon allotropes.^[1a,10a,14] GR possesses a high mobility of charge carriers at room temperature ($200\,000\text{ cm}^2\text{ V}^{-1}\text{ S}^{-1}$) and exhibits an extremely high theoretical specific surface area ($\approx 2600\text{ m}^2\text{ g}^{-1}$),^[15] thus GR-based photocatalysts have been extensively applied to the photo-catalytic degradation of organic compounds.^[14d,16] GO is often used as a precursor of GR in the preparation of GR-based photocatalysts that would have oxygenated functional groups even after the reduction process. These functional groups would favour the formation of a chemical bond between GR and TiO_2 and promote the dispersion of nanoparticles.^[14c,16b,d] Zhang et al. thus claimed that GR- TiO_2 exhibited better photo-catalytic degradation of methylene blue (MB) than that of CNT- TiO_2 with the same carbon content.^[14d] Conversely, Zhang et al.^[1a,10a] and Yang et al.^[17] performed studies on GR-, CNT- and C_{60} - TiO_2 products and reported that there was no advantage of using GR over that of using other forms of carbon in photocatalysis. Evidently, the effects of different carbon materials on TiO_2 photo-degradation are still uncertain; thus there is a pressing need to launch a systematic study on carbon- TiO_2 nanocomposites to clarify the role of carbon materials for photocatalysis.

Herein, we conducted a comparative study on the photocatalytic performance of TiO_2 -based composites containing different types of carbon components in the degradation of rhodamine B (RhB) dye. The AC-, GR-, CNT- and C_{60} - TiO_2 nanocomposites were prepared with the same amount of carbon. Our results showed that these nanocomposites showed enhanced photocatalytic activity compared with that of pure TiO_2 . We propose that it was the excellent adsorption properties, chemical bond formation, enhanced visible-light harvesting, improved dispersion and prolonged lifetime of the charge carriers of these carbon- TiO_2 catalysts that promoted photocatalysis. We also found that GR, CNT and C_{60} could act as electron acceptors to slow down the recombination rate of electron-hole pairs, but the same was not true of AC. The three crystalline carbon materials had essentially no differences in their photocatalytic performance in the degradation of RhB. This study provides a general guideline to design carbon-based photocatalysts through the systematic determination of electronic structures, optical properties and adsorption capabilities.

Results and Discussion

Phase structures and morphology

Figure 1a shows the XRD patterns of the raw C_{60} , CNT, GO and AC precursors before sample preparation. The sharp peaks appearing in the C_{60} curve (top curve) matched well with PDF-#44-0558. The pattern of the CNT contained a typical graphite

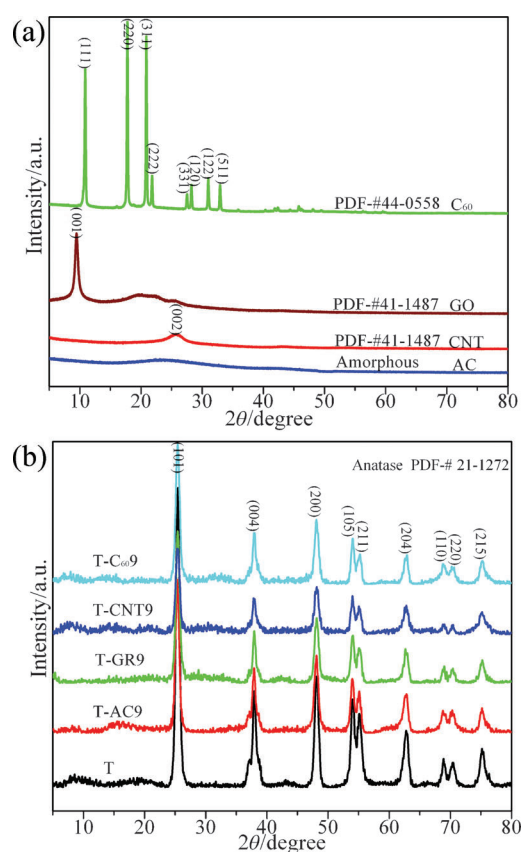


Figure 1. XRD patterns of (a) the carbon precursors and (b) samples of anatase with carbon materials.

peak located at 25.7° , which corresponded to diffraction from the (002) crystalline plane (PDF-#41-1487), whereas GO exhibited one peak located at $2\theta = 9.42^\circ$, which corresponded to the (001) plane.^[18] The oxygen functional group in GO had an enlarged the lattice spacing.^[18b,19] As illustrated by its XRD pattern in Figure 1a (bottom), the absence of the characteristic peak indicated that the AC sample was amorphous. The XRD patterns of the TiO_2 and T-AC9, T-GR9, T-CNT9 and T- C_{60} 9 nanocomposites are shown in Figure 1b. The diffraction patterns could be assigned to the anatase phase (PDF-#21-1272). There were no observable peaks from the carbon components. For the T-GR9 sample, the (001) peak of GO might have been shifted to 25.7° owing to the reduction of the oxygenated group during the solvothermal process,^[14d] and it overlapped with the (101) peak of TiO_2 at 25.4° .^[10b,20] This was a good indication that GO had been reduced to GR successfully during the solvothermal process. The pattern of the T- C_{60} 9 sample did not contain any peak that could be assigned to C_{60} , because the trace content of carbon might have been too small for XRD detection, in agreement with the literature.^[17] Because the AC was amorphous, it was reasonable to observe the sole TiO_2 peaks in the patterns of the T-AC9 sample. The size of the crystals in the samples was estimated from the Scherrer formula by using the peak located at 25.4° in the patterns of samples T, T-AC9, T-GR9, T-CNT9 and T- C_{60} 9. The sizes of the corresponding crystals in the samples were 11.8, 11.4, 11.2, 10.3 and 10.7 nm, re-

spectively. The above results indicated that the incorporation of carbon materials could inhibit the aggregation of primary particles by providing dispersive nucleation sites for TiO₂, which led to smaller particle sizes in the samples. Moreover, it was evident that the introduction of carbon materials into TiO₂ promoted the dispersion of the TiO₂ nanoparticles.^[13]

A TEM image of a typical two-dimensional GRO thin sheet is shown in Figure 2a. Figure 2b shows a TEM image of uniformly distributed TiO₂ particles with a size of about 12 nm; this

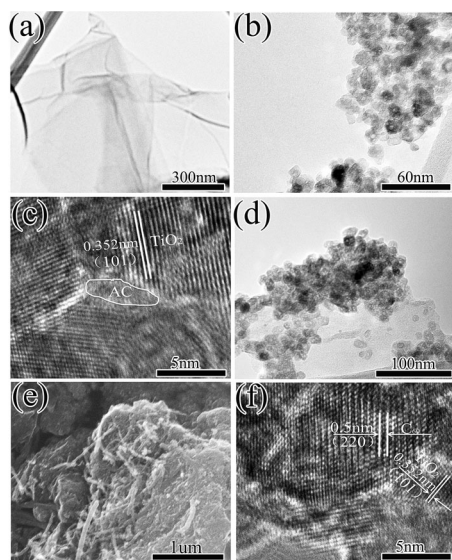


Figure 2. TEM images of (a) GO, (b) T, (c) T-AC9 and (d) T-GR9. e) A SEM image of the T-CNT9 sample. f) A high-resolution TEM (HRTEM) image of T-C₆₀9 sample.

value was consistent with calculations from the XRD results. A combination of AC and TiO₂ nanoparticles was observed, as shown in Figure 2c. Owing to the crystalline structure of TiO₂ and the amorphous phase of AC, the interface of the two components could be easily distinguished, although they appeared to have an intimate contact with each other. Figure 2d presents the TEM image of T-GR9, showing that the TiO₂ nanoparticles were attached to a GR sheet. Figure 2e shows a SEM image of TiO₂ with CNTs. The CNTs were attached onto the surface of the TiO₂ particles. A HRTEM image of TiO₂-C₆₀ is shown in Figure 2f. The larger lattice spacing of 0.5 nm was assigned to the (220) plane of C₆₀, whereas the smaller one of 0.352 nm was assigned to the (101) plane of crystal TiO₂. An intimate interface was formed between C₆₀ and TiO₂. These results indicated that the incorporation of AC, GR, CNT and C₆₀ onto TiO₂ was successful and the samples obtained showed the intimate combination of TiO₂ and the carbon materials.

Surface property

The surface states of the carbon materials and the fabricated composites were elucidated by Raman spectroscopy (RS). As shown in Figure 3a, the RS pattern of CNT contained typical D ($\tilde{\nu}$ = 1351 cm⁻¹) and G peaks ($\tilde{\nu}$ = 1582 cm⁻¹),^[20–21] whereas the

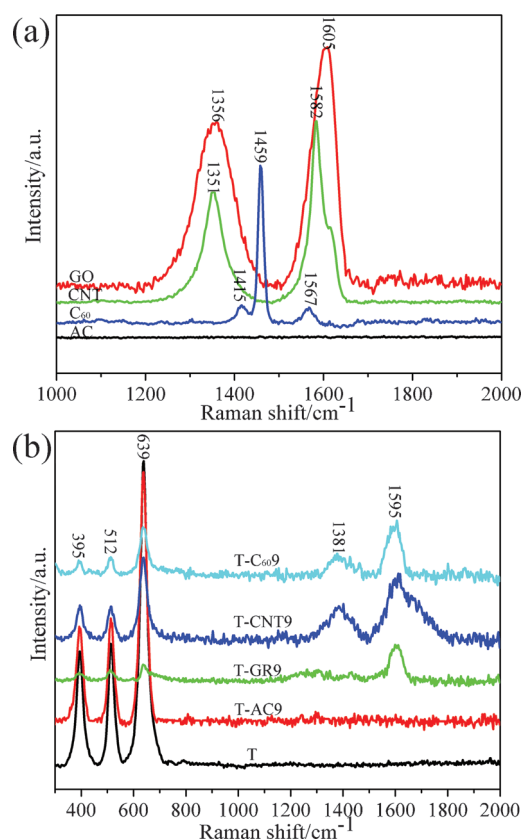


Figure 3. Raman spectra of (a) the carbon materials and (b) samples of anatase with carbon materials.

corresponding two peaks of GO were located at $\tilde{\nu}$ = 1356 and 1605 cm⁻¹; these values are consistent with those reported in the literature.^[22] The RS pattern of C₆₀ featured peaks at $\tilde{\nu}$ = 1415, 1459, and 1567 cm⁻¹,^[23] whereas AC was inactive in RS (Figure 3a, bottom spectrum). For the RS patterns of the TiO₂-based composites, the results are shown in Figure 3b. Three sharp peaks were located at $\tilde{\nu}$ = 395 (B1g), 512 (A1g), and 639 cm⁻¹ (Eg) on the left side of the RS spectra. These peaks were associated with the anatase crystal.^[16d,21,24] The T-GR9, T-CNT9 and T-C₆₀9 samples all showed two peaks located at about $\tilde{\nu}$ = 1381 and 1595 cm⁻¹, which could be assigned as the graphite peak. However, compared with Raman peaks of GO, CNT and C₆₀, remarkable shifts were observed in the composites.^[16a,25] The Raman shift of three crystalline carbon materials indicated that the synergistic effect had taken place upon the addition of carbon materials onto TiO₂. It was also possible that the TiO₂ particles might have induced internal stresses on the carbon components, which resulted in the Raman shift.^[25] Thus, based on the RS results, we conclude that there were interactions between the carbon materials and the TiO₂ phase.

The chemical states on the surface of the prepared samples were investigated by X-ray photo-electron spectroscopy (XPS). Figure 4a shows the C 1s XPS spectra of T, T-AC9, T-GR9, T-CNT9 and T-C₆₀9. The deconvolution of C 1s core-level spectra demonstrated that there were four types of carbon bond in the catalyst products. For sample T without the addition of carbon materials, the peaks located at 284.8, 285.9, 286.7 and

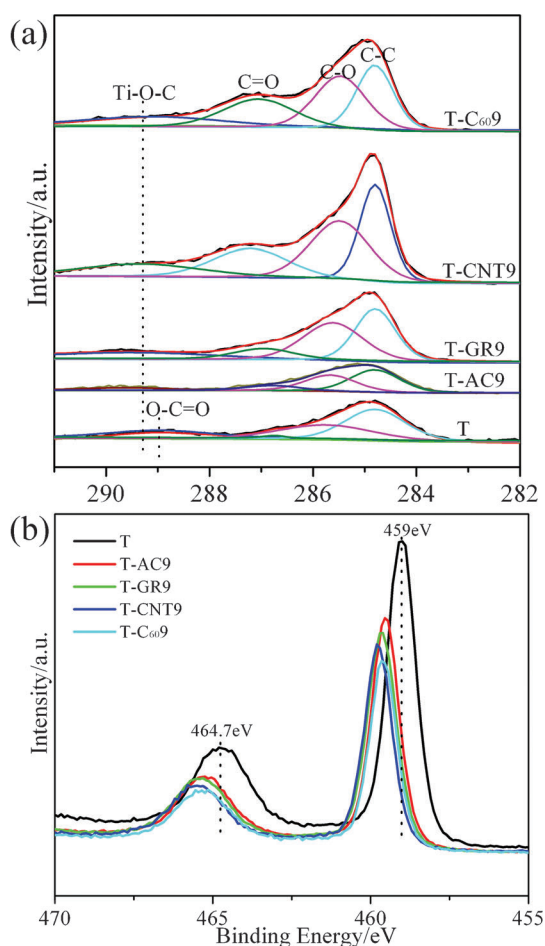


Figure 4. XPS spectra of (a) C 1s and (b) Ti 2p of the composites.

288.8 eV could be assigned to C=C/C–C, C–O, C=O and O–C=O, respectively.^[5c, 16a, d, 22] The presence of carbon was probably due to the adsorption of CO₂ in air while handling the sample. For comparison, composites with carbon components had a new peak centred at 289.3 eV, which indicated the formation of Ti–O–C.^[5b, c, 25–26] The intensity of the 289.3 eV peak was relatively weak in the T-AC9 spectrum. Even after the solvothermal reduction, carbon–TiO₂ composites still contained some oxygenated functional groups, which act as a bridge to connect TiO₂ and carbon materials. Thus, some titanium atoms might be substituted by carbon, so that the Ti–O–C peak could be observed.^[5b] This could further be demonstrated by the Ti 2p XPS spectra shown in Figure 4b. There were two main peaks (459 and 464.7 eV) in the Ti 2p region in the spectrum of sample T, which should be ascribed to 2p_{3/2} and 2p_{1/2} spin-orbital splitting photo-electrons, respectively. The splitting between the 2p_{3/2} and 2p_{1/2} core levels was about 5.7 eV; this indicated the predominant formation of the Ti⁴⁺ state.^[27] The same analysis was applied to samples T-AC9, T-GR9, T-CNT9 and T-C₆₀9 and suggested that Ti⁴⁺ was the overall state in the composites. A notable shift to a higher binding energy for the Ti 2p peaks was observed upon the incorporation of carbon materials; this indicated that the spreading of electron cloud was reduced owing to the formation of Ti–O–C. If the carbon

element with high electronegativity substituted the titanium atom, it would definitely attract the electron cloud from the titanium atom and lead to an observable shift in the XPS pattern.^[5b, c] A similar observation was reported by Chen et al.^[28]

Optical property

UV-visible spectroscopy was employed to explore the light-absorption properties of samples T, T-AC9, T-GR9, T-CNT9 and T-C₆₀9. The results are illustrated in Figure 5. The redshift of the absorption edges was observed upon comparison with sample T. This phenomenon suggested that the

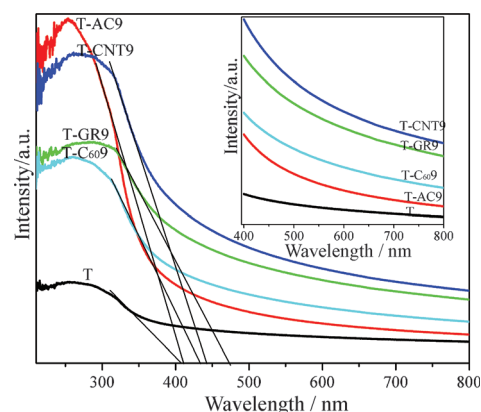


Figure 5. UV-visible absorption spectra of the fabricated composites.

band gap of the composites containing the carbon phase had been narrowed. The inset in Figure 5 shows an enlargement of the visible-light absorption spectra for the products. It was evident that there was a stronger visible-light absorption from the samples incorporating carbon materials.^[29] Based on the above observation, it is reasonable to claim that the chemical interactions had been induced between the carbon materials and TiO₂, as already confirmed by TEM, RS and XPS results. The functional groups (C–O, C=O) were partly reduced during the solvothermal process; thus leaving unpaired π electrons that could be easily bonded to titanium. These chemical interactions occurred over the surface of T-AC9, T-GR9, T-CNT9 and T-C₆₀9 and facilitated the formation of the Ti–O–C bond and narrowed the band gaps of the composites, as in the case of carbon doping in other studies.^[14c, 26] This explains why the efficiency of visible-light adsorption was improved in the TiO₂ samples after the incorporation of AC, GR, CNT and C₆₀.

Photo-luminescence (PL) spectroscopy is known to be a powerful tool to investigate the separation rate of electron–hole pairs in semiconductors. As shown in Figure 6, the PL emission intensities for samples T-AC9, T-GR9, T-CNT9 and T-C₆₀9 were lower than that of pure TiO₂. This indicated that a slower recombination rate was obtained in the samples with carbon components. Furthermore, the emission spectra should be ascribed to surface defects of the composites because the wavelength of the emission peak located at $\lambda = 640\text{--}660$ nm was much longer than that of the near-band-edge emission

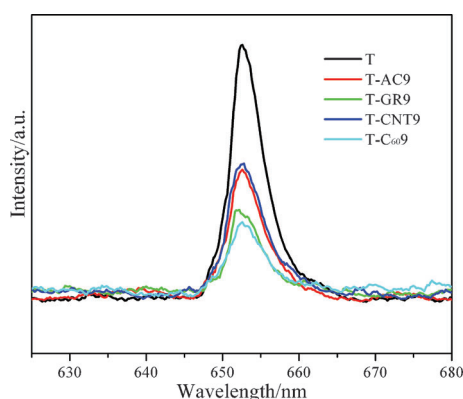


Figure 6. PL spectra of the composites.

peak.^[8f] Thus, the addition of carbon materials to TiO₂ would effectively reduce the surface defects and slow down the recombination rate of electron–hole pairs in the samples.^[22,30] For sample T-AC9, the improvement in the separation rate of electron–hole pairs might be due to the high conductivity of AC, which favours electron transfer. Moreover, highly conductive GR, CNT and C₆₀ could act as sinks for electrons; thus facilitating the separation of electrons and holes. Photo-generated electron would be easily transported to the surface of GR, CNT and C₆₀, and the recombination of electron–hole pairs would be hindered.^[12,31]

Photo-catalysis

RhB dye is often employed in the evaluation of the performance of catalysts for photo-catalytic degradation in water treatment.^[7] A comparative study of dye degradation over the fabricated composites by photo-catalysis is shown in Figure 7. To exclude the possibility of photo-sensitisation of the dye itself, a control experiment without catalyst was also performed. The flat degradation curve (Figure 7, top curve) suggested that the self-degradation of the RhB dye was negligible. To evaluate the effect of carbon content on TiO₂ photo-catalytic performance, a series of T-GR catalysts with different carbon

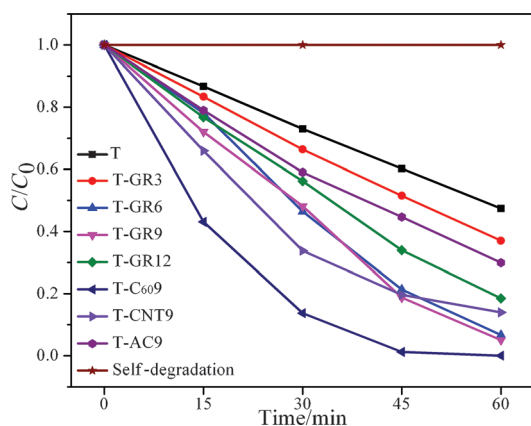


Figure 7. Photo-catalytic degradation of RhB under visible-light irradiation by using the fabricated composites.

contents were prepared and examined under visible-light irradiation. The results showed that a large improvement in the rate of degradation was observed upon the addition of GR. Specifically, the removal efficiencies after irradiation for 60 min for samples T and T-GR9 were 50 and 95 %, respectively. Thus, sample T-GR9 exhibited the optimal photo-catalytic activity. However, the addition of excessive GR to TiO₂ had a negative effect on its catalytic performance. This could be ascribed to the reduction of the surface of TiO₂ exposed to light irradiation.^[1a] Furthermore, optimal ratios of AC, CNT and C₆₀ were doped onto TiO₂ to compare the effect of different carbon materials on TiO₂. The photo-catalytic activity followed the order T-C₆₀9 > T-CNT9 > T-GR9 > T-AC9 > T. To further evaluate the photo-catalytic performance of the composites with carbon materials, the kinetic rate constant was determined by the Langmuir–Hinshelwood model.^[22] For low-concentration pollutants, the pseudo-first-order kinetic model can be adopted, according to following Equations (1) and (2):

$$r = -\frac{dC}{dt} = k_a C \quad (1)$$

$$\ln\left(\frac{C_0}{C}\right) = k_a t \quad (2)$$

in which r is the reaction rate (in mg L⁻¹ min⁻¹), C is concentration of pollutant (in mg L⁻¹), C_0 is the adsorption equilibrium concentration of pollutant (in mg L⁻¹), t is reaction time (in min) and k_a is the apparent rate constant (in min⁻¹). Table 1 shows the k_a values of catalysts T, T-AC9, T-GR9, T-CNT9 and T-C₆₀9 under visible-light irradiation. It was evident that AC, GR, CNT and C₆₀ could promote TiO₂ photo-catalytic degradation of

Table 1. Reaction rate constants (k_a) for the photo-catalytic degradation of RhB under visible-light irradiation.^[a]

	T	T-AC9	T-GR9	T-CNT9	T-C ₆₀ 9
k_a [min ⁻¹]	0.01173	0.01897	0.02388	0.03558	0.06424
R^2	0.9936	0.9943	0.99738	0.9951	0.9941

[a] R^2 represents the square of the correlation coefficient for kinetic linear fitting.

RhB, whereas T-GR9, T-CNT9 and T-C₆₀9 presented better photo-catalytic performances compared with T-AC9. Meanwhile, T-C₆₀9 provided the most rapid photo-catalytic activity, followed by T-CNT9 and T-GR9 in our studies. Therefore, GR did not seem to have an advantage in the photo-catalytic degradation of RhB, compared with those of CNTs and C₆₀.

To explain the enhanced effects of the carbon components on TiO₂ photo-catalytic degradation, our interpretations were based on the results of characterisation. First, the introduction of carbon materials into TiO₂ enhanced the adsorption ability for the organic dye. As illustrated in Figure 8, the adsorption experiment performed in the dark showed that catalysts with carbon components had better adsorption performances than

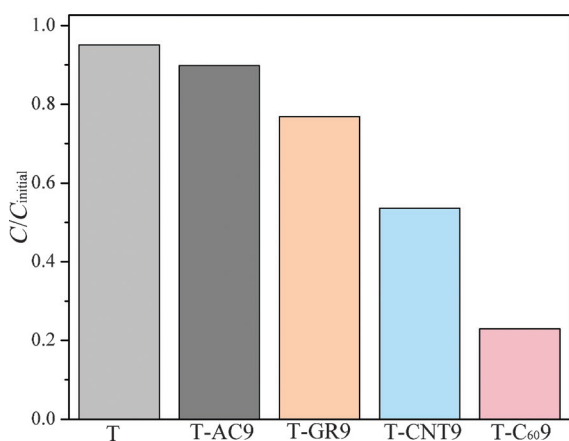


Figure 8. Histogram showing the adsorption abilities of the RhB organic dye for the samples after 15 min in the dark.

that of the same amount of pure TiO_2 . Easy access to pollutants would enhance photo-catalysis on the surface of the samples. The best adsorption ability of T-C₆₀9 for RhB might originate from the smaller C₆₀ particle size (Figure S3 in the Supporting Information) and its good dispersion in the nanocomposite. Second, the intimate contact between the TiO_2 particles and the carbon materials would result in smaller particle sizes and assure uniform distribution; thus providing more active sites for photo-catalysis and the degradation of the dye molecules. Third, chemical bond formation (Ti–O–C), as verified by RS, XPS and UV-visible spectroscopy, narrowed the band gap of the composites, which promoted visible-light harvesting and generated electron–hole pairs. Fourth, the effective separation of photo-generated electron–hole pairs was achieved upon the addition of carbon material, as illustrated by the PL results. The overall improved photo-catalytic performance of carbon– TiO_2 nanocomposites compared with that of bare TiO_2 resulted from a synergistic effect of these key factors.

Furthermore, photo-catalytic mechanisms were also proposed based on the above analysis. It was reported that the work function of the RhB molecule and excited RhB were 5.45 and 3.08 eV, respectively.^[16b] The electron affinity of anatase TiO_2 is 4.2 eV,^[16d,22] which is higher than that of the work function of excited RhB. By considering that the absorption edge of samples T and T-AC9 (though its absorption edge had been redshifted) were both located lower than $\lambda = 420$ nm (the cutoff filter of the irradiation used in this study), the observed photo-catalytic activity should be attributed to the photo-sensitisation of RhB. As shown in Figure 9a, under visible-light irradiation, RhB could be photo-excited to the RhB* state and the resulting electron would be energetically favourably transferred to the conduction band of TiO_2 and would achieve separation of electron–hole pairs. Meanwhile, if RhB* was converted into the cationic

radical (RhB^{•+}), the separated electron would be captured by surface oxygen to produce reactive oxygen radicals; thereafter, the RhB molecules would be degraded by these reactive radicals. In the case of T-AC9, the incorporation of AC sped up the charge-carrier transfer rate, which had a positive effect on photo-catalysis. For T-GR9, T-CNT9 and T-C₆₀9, the band gaps were narrowed and could be activated under visible-light irradiation. In addition, GR, CNT and C₆₀ were reported to be effective electron sinks because their corresponding work functions were 4.4, 4.8 and 4.3 eV,^[3,13,16d,22,32] respectively. As illustrated in Figure 9b, a photo-excited electron both from RhB and T-GR9, T-CNT9 and T-C₆₀9 would be transported to the GR sheet, CNTs and C₆₀, respectively, owing to their energy band structures. In addition to the reactive radicals produced according to the suggested pathway illustrated in Figure 9a, the resultant hole would also combine with surface OH^- or H_2O to form $\cdot\text{OH}$ radi-

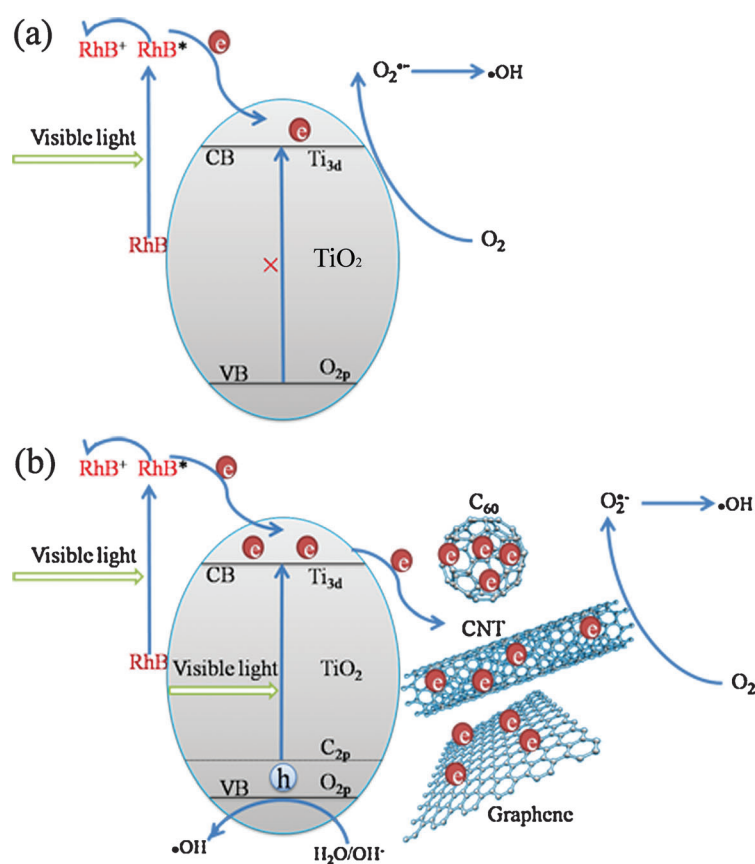


Figure 9. Proposed mechanisms for the photo-catalytic degradation of RhB over the catalyst. VB = valence band.

icals. Thus, it was not surprising to observe remarkably promoted photo-catalytic degradation properties when using T-GR9, T-CNT9 and T-C₆₀9, compared with those of T and T-AC9. To confirm the proposed mechanism, the $\cdot\text{OH}$ groups were recorded in catalyst T-C₆₀9 at different times. As shown in Figure 10, $\cdot\text{OH}$ was released incrementally with increasing reaction time. The inset in Figure 10 exhibits the time dependence of the PL intensity. The linear relationship indicated that the

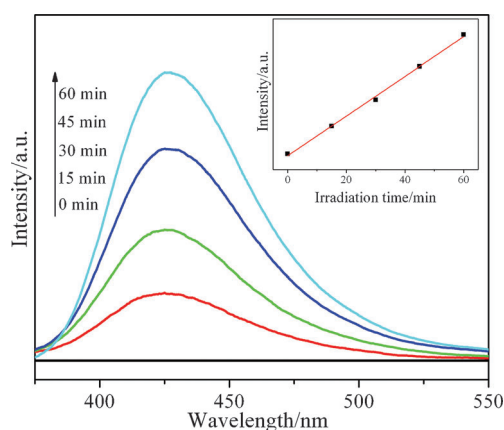


Figure 10. PL spectral changes taken from basic TA solution under visible-light irradiation over T-C₆₀9. Inset: the corresponding PL intensity measured from the $\lambda = 426$ nm peak versus irradiation time.

rate of release of $\cdot\text{OH}$ in T-C₆₀9 was stable, which also matched well with the kinetic analysis described in Table 1. Therefore, the proposed mechanisms could well elucidate the photo-catalytic activity of as-prepared composites. GR, CNT and C₆₀, with excellent adsorption abilities and conductivity, would all serve as electron sinks in promoting TiO₂ photo-catalytic degradation of RhB from the above analysis. T-AC9, without an electron trap (AC could not serve as electron sink), showed weaker interactions between AC and TiO₂, a lower rate of adsorption to the dye and a larger band gap; this led to a relatively low photo-catalytic property, compared with that of T-GR9, T-CNT9 and T-C₆₀9. In addition, T-C₆₀9 showed the best photo-catalytic performance relative to T-GR9 and T-CNT9, which could be attributed to the strongest interaction of carbon and TiO₂, the largest adsorption capability for RhB and most effective separation of photo-induced charge carriers.

In industrial applications, it is important that a catalyst is chemically stable and can be used repeatedly. In the evaluation of the stability of T-C₆₀9, the sample was directly immersed into pollutant solution each time without being washed after the former run finished. Figure 11 shows the degradation efficiency of T-C₆₀9 after 60 min under visible-light irradiation for

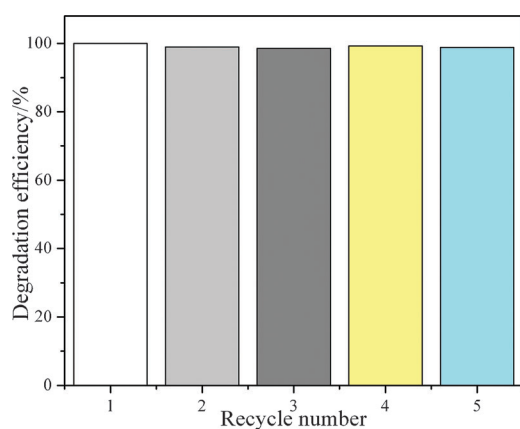


Figure 11. The photo-catalytic performance of catalyst T-C₆₀9 in repeated cycles.

five runs. Even after five runs, a negligible decrease in photo-catalytic performance was observed; this indicated that T-C₆₀9 was re-usable and had an excellent stability for the photo-catalytic degradation of RhB.

Conclusion

AC-, GR-, CNT- and fullerene-TiO₂ nanocomposites were successfully prepared by a solvothermal method combined with post-annealing treatment. The incorporation of carbon materials onto TiO₂ enhanced its photo-catalytic degradation of RhB owing to the high adsorption ability for the dye, improved dispersion of active sites, enhanced visible-light harvesting with a narrower band gap and effective separation of electron-hole pairs. This study offers general guidelines for designing photo-catalysts with carbon components.

Experimental Section

Sample preparation

The raw precursors GO, AC, CNT and C₆₀ were purchased from the Nanjing XFNANO Materials Tech Company. GO was dispersed evenly in anhydrous ethanol by using ultrasound to achieve a uniform concentration of 1 mg mL⁻¹ before use in sample preparation. CNTs and C₆₀ (as shown in Figures S2 and S3 in the Supporting Information) were both pre-treated in concentrated HNO₃ (68%) at 130 °C for 4 h, whereas AC (as shown in Figure S1 in the Supporting Information) was treated with concentrated HNO₃ (68%) at 60 °C for 2 h to avoid over-oxidation. Titanium(IV) *n*-butoxide (TBOT; 99%, Acros) was used as a precursor for titania. Acetic acid (HAC; 100%, analytic purity) served as an inhibitor to control the rate of hydrolysis of TBOT. Distilled water with a resistivity of 18 M Ω cm⁻¹ was used in these experiments. Carbon-TiO₂ composites were synthesised by a solvothermal method followed by a post-heating treatment. In a typical preparation of a GR-TiO₂ sample, TBOT (3 mL), HAC (7 mL) and GO (3, 6, 9, or 12 mg) were placed in anhydrous ethanol (20 mL) and mixed under magnetic stirring for 1 h. Distilled water (5 mL) was added dropwise to the mixture before it was transferred to a 45 mL stainless-steel autoclave for heating at 180 °C for 10 h. The precipitate in the mixture was collected by centrifugation (with 3000 rpm) and was washed with anhydrous ethanol. The grey powder was dried at 80 °C for 6 h before calcination at 400 °C for 2 h in argon. The final GR-TiO₂ products, labelled as T-GR3, T-GR6, T-GR9, and T-GR12, corresponded to 0.4, 0.8, 1.25 and 1.65 wt% carbon, respectively. For the preparation of AC-, CNT- and C₆₀-TiO₂ composites, 9 mg of AC, CNT and C₆₀ was used instead and samples prepared with the same procedure as described above. The samples were referred to as T-AC9, T-CNT9 and T-C₆₀9, respectively. As a control, a nanocrystalline sample of TiO₂ was also prepared and denoted by T.

Characterisation

XRD analysis was conducted by using a Rigaku RU300 diffractometer with Cu α radiation ($\lambda = 0.1540598$ nm). Electron microscopy was performed by using a Quanta F400 field-emission scanning electron microscope and a Tecnai G² 20S-Twin 120 kV transmission electron microscope. The UV/Vis absorption spectra were obtained by using a Hitachi UV/Vis spectrophotometer (U-3501). PL spectra were recorded by using a Hitachi F-4500 fluorescence spectrophoto-

tometer with an excitation wavelength of $\lambda = 325$ nm. XPS was performed by using a PHI Model 5802 instrument with $Al_{K\alpha}$ radiation and calibrated with C 1 s at 284.8 eV.

Photo-catalysis

The photo-catalytic performance of the samples was evaluated by observing their abilities to degrade the RhB dye in aqueous solutions under visible-light irradiation induced by a 300 W Xe lamp (HSX-F300, Beijing NBET Technology) with a $\lambda = 420$ nm cutoff filter. The reaction chamber was placed under the light beam at a distance of 20 cm. In a typical evaluation procedure, sample (50 mg) was placed into the RhB solution (50 mL at a concentration of 5 mg L^{-1}). The suspension was stirred for 30 min in the dark to achieve adsorption equilibrium between RhB dye and the sample before it was placed in the reaction chamber for visible-light exposure. At a given time interval, 1.5 mL of the solution was collected and the concentration of RhB was determined by measuring the light absorbance of RhB at $\lambda = 553$ nm by means of UV/Vis spectroscopy. In this experiment, the RhB concentration immediately after adsorption equilibrium in the dark was denoted by C_0 . To confirm the presence of $\cdot\text{OH}$, PL spectroscopy was employed. The approach was similar to those used by Liu et al.,^[33] who used terephthalic acid (TA) molecules as a probe. In the analysis, (20 mg) catalyst was dispersed into a mixture (20 mL) of TA (3 mmol L^{-1}) and NaOH (10 mmol L^{-1}) under stirring in the dark for 30 min before visible-light irradiation. At a given time interval, 2 mL of sample was collected to monitor the concentration of $\cdot\text{OH}$ by measuring the PL peak intensity of the 2-hydroxyterephthalic acid generated at $\lambda = 426$ nm by using a Hitachi F-4500 fluorescence spectrophotometer with an excitation wavelength of $\lambda = 320$ nm.

Acknowledgements

This study is supported by the Direct Grant for Research 2011/2012 from the Faculty of Science, The Chinese University of Hong Kong (Project code: 2060439).

Keywords: carbon · dyes/pigments · fullerenes · graphene · photochemistry · titanium

- [1] a) Y. Zhang, Z.-R. Tang, X. Fu, Y.-J. Xu, *ACS Nano* **2010**, *4*, 7303–7314; b) H. B. Wu, H. H. Hng, X. W. Lou, *Adv. Mater.* **2012**, *24*, 2567–2571.
- [2] a) W. Liang, T. L. Church, A. T. Harris, *Green Chem.* **2012**, *14*, 968–975; b) J. B. Joo, Q. Zhang, M. Dahl, I. Lee, J. Goebel, F. Zaera, Y. D. Yin, *Energy Environ. Sci.* **2012**, *5*, 6321–6327; c) J. B. Joo, Q. Zhang, I. Lee, M. Dahl, F. Zaera, Y. Yin, *Adv. Funct. Mater.* **2012**, *22*, 166–174.
- [3] Y. Long, Y. Lu, Y. Huang, Y. Peng, Y. Lu, S.-Z. Kang, J. Mu, *J. Phys. Chem. C* **2009**, *113*, 13899–13905.
- [4] O. Akhavan, R. Azimirad, S. Safa, M. Larijani, *J. Mater. Chem.* **2010**, *20*, 7386–7392.
- [5] a) L. Zhang, M. S. Tse, O. K. Tan, Y. X. Wang, M. Han, *J. Mater. Chem. A* **2013**, *1*, 4497–4507; b) J. Yu, G. Dai, Q. Xiang, M. Jaroniec, *J. Mater. Chem.* **2011**, *21*, 1049–1057; c) H. Wang, Z. Wu, Y. Liu, *J. Phys. Chem. C* **2009**, *113*, 13317–13324.
- [6] J. Zhang, C. Pan, P. Fang, J. Wei, R. Xiong, *ACS Appl. Mater. Interfaces* **2010**, *2*, 1173–1176.
- [7] W. Zhou, Z. Yin, Y. Du, X. Huang, Z. Zeng, Z. Fan, H. Liu, J. Wang, H. Zhang, *Small* **2013**, *9*, 140–147.
- [8] a) Q. Xiang, J. Yu, B. Cheng, H. Ong, *Chem. Asian J.* **2010**, *5*, 1466–1474; b) Y. Lu, H. Yu, S. Chen, X. Quan, H. Zhao, *Environ. Sci. Technol.* **2012**, *46*, 1724–1730; c) Q. Zhang, D. Q. Lima, I. Lee, F. Zaera, M. Chi, Y. Yin, *Angew. Chem.* **2011**, *123*, 7226–7230; ; *Angew. Chem. Int. Ed.* **2011**, *50*, 7088–7092; d) A. Furube, L. Du, K. Hara, R. Katoh, M. Tachiya, *J. Am. Chem. Soc.* **2007**, *129*, 14852–14853; e) Y. Tian, T. Tatsuma, *J. Am. Chem. Soc.* **2005**, *127*, 7632–7637; f) Q. Deng, X. Duan, D. H. Ng, H. Tang, Y. Yang, M. Kong, Z. Wu, W. Cai, G. Wang, *ACS Appl. Mater. Interfaces* **2012**, *4*, 6030–6037.
- [9] H. Yang, Z. Tan, Y. Liu, Z. Ma, L. Zhang, *IEEE Trans. Nanotechnol.* **2013**, *12*, 1037–1041.
- [10] a) Y. Zhang, Z. R. Tang, X. Fu, Y. J. Xu, *ACS Nano* **2011**, *5*, 7426–7435; b) Q. Li, H. Yang, A. Nie, X. Fan, X. Zhang, *Catal. Lett.* **2011**, *141*, 1237–1242; c) Q. Li, H. Yang, F. Qiu, X. Zhang, *J. Hazard. Mater.* **2011**, *192*, 915–921.
- [11] Q. Li, H. Yang, Z. Ma, X. Zhang, *Catal. Commun.* **2012**, *17*, 8–12.
- [12] K. Woan, G. Pyrgiotakis, W. Sigmund, *Adv. Mater.* **2009**, *21*, 2233–2239.
- [13] Y.-J. Xu, Y. Zhuang, X. Fu, *J. Phys. Chem. C* **2010**, *114*, 2669–2676.
- [14] a) N. Yang, Y. Liu, H. Wen, Z. Tang, H. Zhao, Y. Li, D. Wang, *ACS Nano* **2013**, *7*, 1504–1512; b) J. Zhang, Z. Zhu, Y. Tang, X. Feng, *J. Mater. Chem. A* **2013**, *1*, 3752–3756; c) J. S. Lee, K. H. You, C. B. Park, *Adv. Mater.* **2012**, *24*, 1133–1133; d) H. Zhang, X. Lv, Y. Li, Y. Wang, J. Li, *ACS Nano* **2010**, *4*, 380–386; e) N. Zhang, Y. Zhang, M.-Q. Yang, Z.-R. Tang, Y.-J. Xu, *J. Catal.* **2013**, *299*, 210–221; f) N. Zhang, M.-Q. Yang, Z.-R. Tang, Y.-J. Xu, *J. Catal.* **2013**, *303*, 60–69; g) Y. Zhang, N. Zhang, Z.-R. Tang, Y.-J. Xu, *ACS Nano* **2012**, *6*, 9777–9789; h) N. Zhang, Y. Zhang, Y.-J. Xu, *Nanoscale* **2012**, *4*, 5792–5813.
- [15] Q. Xiang, J. Yu, M. Jaroniec, *Chem. Soc. Rev.* **2012**, *41*, 782–796.
- [16] a) B. Cai, X. Lv, S. Gan, M. Zhou, W. Ma, T. Wu, F. Li, D. Han, L. Niu, *Nanoscale* **2013**, *5*, 1910–1916; b) J. Zhang, Z. Xiong, X. Zhao, *J. Mater. Chem.* **2011**, *21*, 3634–3640; c) H. Zhang, X. Fan, X. Quan, S. Chen, H. Yu, *Environ. Sci. Technol.* **2011**, *45*, 5731–5736; d) Y. Wen, H. Ding, Y. Shan, *Nanoscale* **2011**, *3*, 4411–4417.
- [17] M.-Q. Yang, N. Zhang, Y.-J. Xu, *ACS Appl. Mater. Interfaces* **2013**, *5*, 1156–1164.
- [18] a) Q. Shou, J. Cheng, L. Zhang, B. J. Nelson, X. Zhang, *J. Solid State Chem.* **2012**, *185*, 191–197; b) H. Yang, L. Zhang, X. Dong, W. Zhu, J. Zhu, B. Nelson, X. Zhang, *Nanotechnology* **2012**, *23*, 065604–065609.
- [19] L. Dong, K. Shou, D. R. Frutiger, A. Subramanian, L. Zhang, B. J. Nelson, X. Tao, X. Zhang, *IEEE Trans. Nanotechnol.* **2008**, *7*, 508–517.
- [20] Q. Li, X. Hou, H. Yang, Z. Ma, J. Zheng, F. Liu, X. Zhang, Z. Yuan, *J. Mol. Catal. A: Chem.* **2012**, *356*, 121–127.
- [21] K. Zhou, Y. Zhu, X. Yang, X. Jiang, C. Li, *New J. Chem.* **2011**, *35*, 353–359.
- [22] P. Wang, Y. Tang, Z. Dong, Z. Chen, T.-T. Lim, *J. Mater. Chem. A* **2013**, *1*, 4718–4727.
- [23] K. Nakamoto, M. A. McKinney, *J. Chem. Educ.* **2000**, *77*, 775–780.
- [24] M. Wojtoniszak, B. Zielinska, X. Chen, R. J. Kalenczuk, E. Borowiak-Palen, *J. Mater. Sci.* **2012**, *47*, 3185–3190.
- [25] Y. L. Min, K. Zhang, W. Zhao, F. C. Zheng, Y. C. Chen, Y. G. Zhang, *Chem. Eng. J.* **2012**, *193*–194, 203–210.
- [26] Y. Zhang, C. Pan, *J. Mater. Sci.* **2011**, *46*, 2622–2626.
- [27] C. Su, L. Liu, M. Zhang, Y. Zhang, C. Shao, *CrystEngComm* **2012**, *14*, 3989–3999.
- [28] L.-C. Chen, Y.-C. Ho, W.-S. Guo, C.-M. Huang, T.-C. Pan, *Electrochim. Acta* **2009**, *54*, 3884–3891.
- [29] P. Gao, D. D. Sun, *Chem. Asian J.* **2013**, *8*, 2779–2786.
- [30] D. Wang, Z. H. Zhou, H. Yang, K. B. Shen, Y. Huang, S. Shen, *J. Mater. Chem.* **2012**, *22*, 16306–16311.
- [31] R. Leary, A. Westwood, *Carbon* **2011**, *49*, 741–772.
- [32] A. Kongkanand, P. V. Kamat, *ACS Nano* **2007**, *1*, 13–21.
- [33] G. Liu, Q. Deng, H. Wang, D. H. L. Ng, M. Kong, W. Cai, G. Wang, *J. Mater. Chem.* **2012**, *22*, 9704–9713.

Received: November 13, 2013

Published online on January 21, 2014